J. Phys. Chem. A **2002,** *106,* 307−311

Kinetics of the Reaction Al + SF_6 in the Temperature Range 499−813 K

James K. Parker, Nancy L. Garland, and H. H. Nelson*

Code 6110, Chemistry Division, Naval Research Laboratory, 4555 Overlook Avenue S.W., Washington, D.C. 20375

Received: July 26, 2001; In Final Form: October 4, 2001

Rate constants as a function of temperature for the reaction Al + SF_6 have been measured under pseudo-first-order conditions. Laser-induced fluorescence was used to monitor the relative concentrations of either the reactant Al or the primary product AlF. The measured rate constants are described by the expression $k(T) = 6.8\ (\pm\ 2.2) \times 10^{-10} \exp(-(4780 \pm 200\ \mathrm{K})/T)\ \mathrm{cm^3\ molecule^{-1}\ s^{-1}}$ over the range 499−813 K. Ab initio and density functional calculations at the MP2(FC) and BH&HLYP levels have been used to model the potential energy surface for this reaction. Calculated rate constants are in good agreement with experimental observations.

Introduction

Aluminum is used as a fuel in some solid rocket motors because of its high energy density, its effect on suppressing combustion instabilities, and because it is a relatively inexpensive and readily available material.[1] There are, however, problems associated with using aluminum in the fuel. $Al_2O_{3(l)}$ slag can accumulate on the nozzle leading to a decrease in the rocket's overall performance, and it is also associated with the formation of smoky exhaust trails. A potential solution to these problems is to add fluorine-containing materials to the aluminized propellant.[2,3] It has been postulated that fluorine will eliminate formation of condensed phase metal oxide products, shorten burn times of aluminum particulate, and enhance metal ignition characteristics in oxygen environments by attacking the aluminum oxide particle coating and lowering ignition temperature. Mass spectrometric studies[3] of the reaction of aluminum and fluorine in oxygen/hydrogen flames have shown that major product species in the flame are AlOF, AlOH, and AlO. In systems where fluorine and oxygen are present, it has been predicted that aluminum oxyfluoride (AlF_2O) will be the dominant final product.[4] This species is a gas at rocket exhaust temperatures.

In order for combustion modelers to have the ability to accurately predict species distributions, a reliable kinetics database is necessary.[5] Currently, gas-phase kinetics data is unavailable for reactions of aluminum with fluorinated compounds, with the exception of NF_3.[6] In this investigation we have undertaken a combined experimental and computational study of the kinetics of the prototype reaction:

$$\mathrm{Al} + \mathrm{SF_6} \rightarrow \mathrm{AlF} + \mathrm{SF_5} \tag{1}$$

Results from this study will be used to guide further investigations in our laboratory.

Experimental Section

Al(^2P) atoms were generated by photolysis[7] of trimethylaluminum (TMA) or triethylaluminum (TEA) at 248 nm, and were monitored by laser-induced fluorescence (LIF) via the $^2S_{1/2} \leftrightarrow {}^2P_{1/2}$ transition near 394.4 nm. A plot of the reciprocal Al chemical lifetime (disappearance rate) vs SF_6 partial pressure yielded the bimolecular rate constant. Each first-order plot of τ^{-1} vs P_{SF_6} contained approximately 10 data points. Each data point on the first-order plot was obtained from a plot of LIF intensity vs time, which contained 500 data points. When TMA was the Al atom precursor, 2 laser shots per data point were averaged; when TEA was the precursor, 8−10 laser shots per data point were averaged. The total pressure in the reactor was maintained at 100 Torr. In one experiment, AlF product concentrations were monitored, by LIF on the $A^1\Sigma \leftrightarrow X^1\Sigma$ transition near 227.5 nm, at varying partial pressures of SF_6. In this experiment, 10 laser shots per data point were averaged.

The stainless steel reactor consists of a 21-cm diameter, double-hulled, spherical main body onto which four 20-cm diameter vacuum flanges are welded. Cooling water flows between the hulls through a series of baffles. The four ports on the sides of the vacuum housing provide optical access for collinear laser beams, for fluorescence collection at right angles, and electrical access for resistive heating. The arms of the reactor are sealed by flanges with copper gaskets. TMA/Ar, TEA/Ar, Ar buffer gas, and SF_6 gases were premixed in 6.4 mm stainless steel tubing about 1 m upstream from the reactor; these gases then flowed directly into the base of the reactor. Because TEA has a low vapor pressure, it was necessary to bubble argon through the liquid, which was heated to approximately 70 °C. The gas lines were held at a temperature of approximately 120 °C with heating tape in order to prevent recondensation of the TEA vapor. A three-way cross on the top of the reactor provides ports for pumping, pressure, and temperature measurements. Gas temperatures were measured with a 13%Pt/Rh thermocouple; pressures were measured with a Baratron (MKS Instruments 627B13TBC1B). The thermocouple temperature was compared with AlO rotational temperatures at 296 and 780 K. In both cases, the temperatures determined by the two methods agreed to within 5%.

A 5.7-cm o.d., 5.1-cm i.d., 30.5-cm long Al_2O_3 reaction tube is situated inside the reactor. Four 1.3-cm holes in the middle of the reaction tube, drilled 16.5-cm from the base, provide optical access. The reaction tube is surrounded by a ceramic-insulated resistor and Al_2O_3 insulation material. The resistor is connected via vacuum electrical feedthroughs to a transformer which provides current for heating.

10.1021/jp012895n CCC: $22.00

The photolysis laser was a Lambda-Physik excimer laser (EMG 201 MSC) operating on KrF. The photolysis beam passed through a 6-mm diameter iris before being directed through the MgF_2 windows of the reactor. The Al chemical lifetime had no dependence on the photolysis pulse energy which varied from 20 to 60 mJ pulse^{-1}. The Al(^{2}P) atoms were probed with the output of a Lambda-Physik excimer pumped dye laser (EMG 102/FL2002) operating with PBBO dye in dioxane. The dye laser and photolysis laser beams were collinear and counter-propagated through the reactor. The fluorescence was focused by a two-lens telescope through an iris onto a filtered photomultiplier tube (PMT) (Burle C31000M). A Corning 5-58 band-pass filter, which transmitted fluorescence of the Al($^2S_{1/2}$) $\leftrightarrow$ Al ($^2P_{1/2}$) transition, was used as well as a 1-cm thick quartz cell of CCl_4 to block scattered photolysis laser light from the photomultiplier tube. For the AlF experiment, a 228 nm band-pass filter was used to transmit fluorescence of the $A^1\Sigma \leftrightarrow X^1\Sigma$ transition near 227.5 nm. In this case, 455 nm laser radiation was passed through a BBO doubling crystal to generate photons at 227.5 nm. The output power at this wavelength was approximately 150 μJ pulse^{-1}.

A programmable digital delay generator (DDG) (SRS DG-535) controlled the timing for the kinetics experiments. The DDG provides trigger pulses at a fixed delay to the photolysis laser and at variable delays simultaneously to the probe laser and the boxcar integrator. A gated boxcar integrator captured the LIF signal and directed it to a computer. The Al and AlF chemical lifetimes were obtained by sequentially increasing the delay between the two laser pulses. All kinetics scans were initiated 5 μs after the photolysis laser trigger to ensure that the Al(^{2}P) and AlF $X^1\Sigma$ would be in thermal equilibrium with the bath gas.

The flow rates of the gases were measured with calibrated mass flow meters (Tylan 2950). For kinetics experiments at 100 Torr and in the temperature range of 499 to 612 K, 500 standard cubic centimeters per minute (sccm) of argon and 30 sccm of 0.1% TMA in Ar were flowed through the inlet tube. A flow of 100 sccm of Ar was directed over the windows to prevent accumulation of metallic aluminum. Above 600 K the aluminum LIF signal strongly decreased to zero in the presence of sulfur hexafluoride. Quenching was ruled out as the cause of signal loss because simply turning off the SF_6 flow did not restore the aluminum LIF signal after several turnovers of gas in the cell. The use of TEA from 638 to 813 K and much faster flow rates partially alleviated this problem. However, an upper limit of 813 K on the temperature was reached due to difficulty maintaining Al LIF signal in the presence of SF_6. When TEA was used, 5.0 standard liters per minute (slpm) of Ar buffer gas and 40 sccm of approximately 0.25% TEA in Ar were flowed through the inlet tube. A flow rate of 100 sccm of argon was maintained over the windows. As SF_6 was added to the system, the partial pressure of the Ar buffer gas was decreased to maintain the total pressure. All kinetics experiments were carried out under pseudo-first-order conditions. Sulfur hexafluoride concentrations were greater than 100 times the concentration of either Al or AlF, ensuring pseudo-first-order conditions.

TMA and TEA were obtained from Akzo Nobel (95% pure, other impurities consisted of higher molecular weight aluminum alkyls). TMA was subjected to several freeze−pump−thaw cycles before use in order to remove volatile impurities such as methane. Ar (Air Products, 99.995%), and SF_6 (Matheson, 99.995%) were used without further purification. The system was calibrated against known rate constants from the Al + CO_2 and Ga + SF_6 reactions.[8,9] The rate constant for the Al + CO_2 reaction was measured at 20 Torr total pressure and 296 K. Our value of 5.7 (± 0.5) × 10^{-13} cm^3 molecule^{-1} s^{-1} is in excellent agreement with the value of 0.60 (±0.05) × 10^{-12} cm^3 molecule^{-1} s^{-1} reported by Garland et al.[9] at 20 Torr and 298 K. The Ga + SF_6 rate constant was measured at 100 Torr and 296 K. Our value of 1.4 (± 0.2) × 10^{-14} cm^3 molecule^{-1} s^{-1} compares reasonably well with the literature value of 8 (± 3) × 10^{-15} cm^3 molecule^{-1} s^{-1}.

Computational Methods

The ab initio and density functional calculations were carried out via the Gaussian 98 suite of programs[10] running on a Silicon Graphics Origin 2000 computer. Geometry optimizations and calculation of normal, harmonic vibrational modes for reactants, products, and transition state structures, were carried out at the BH&HLYP/6-31G(d), BH&HLYP/6-311++G(2d), MP2(FC)/6-31G(d), and MP2(FC)/6-311++G(2d) levels of theory.[11−17] Single-point energies were computed using the aug-cc-pVTZ basis set[18] for all stationary points at the BH&HLYP/6-311++G(2d) and MP2(FC)/6-311++G(2d) levels of theory. The unrestricted MP2 method was used on species with doublet spin multiplicity. Accordingly, all MP2 relative energies in this paper have been determined utilizing the UMP2 electronic potential energies. For calculations on species with doublet spin multiplicity, the value of $\langle S^2 \rangle$ prior to annihilation is less than 0.77, indicating that these species are well-described by a single determinant wave function.[19]

Canonical transition state theory[20,21] was used to predict rate constants for these reactions within the temperature range studied by experiment. The rate constants, $k(T)$, were computed with the following expression:

$$k(T) = \frac{k_b T}{h}\frac{Q^{TS}}{Q^{Al}Q^{SF_6}}\exp\left(\frac{-\Delta E_a}{k_b T}\right) \qquad (2)$$

Here Q^{TS}, Q^{Al} , and Q^{SF_6} are the total computed partition functions (including rotational symmetry numbers, where appropriate) for the transition state, Al atom, and SF_6 molecule at temperature T, ΔE_a is the activation energy including zero-point vibrational correction and thermal corrections to the enthalpy, k_b is Boltzmann's constant, and h is Plank's constant. In computing the electronic function for the aluminum atom, the multiplicity of the states $^2P_{3/2}$ and $^2P_{1/2}$ and the energy gap[22] of 112.06 cm^{-1} have been taken into consideration.

Results

Figure 1 shows typical temporal decay profiles for Al(^{2}P) LIF signal generated using TMA and TEA precursors. The signal-to-noise ratio in experiments where TMA was used as the Al atom precursor is much higher than for those experiments involving TEA. Consequently, the number of laser shots per data point was increased from 2 in the TMA experiments to 8−10 in the TEA experiments. The main factors contributing to the aluminum atom disappearance rate in the absence of added SF_6 are reaction with unphotolyzed TMA and diffusion. The reaction rate constant of Al + TMA at 296 K is reported[23] to be 1.3 (±0.3) × 10^{-10} cm^3 molecule^{-1} s^{-1}. We also measured a value of 1.3 (± 0.1) × 10^{-10} cm^3 molecule^{-1} s^{-1} for this rate constant at 296 K using the same assumptions (i.e., dimerization of TMA neglected) as the investigators of ref 23. At room temperature, all Al LIF decay curves were single exponential. At higher temperatures, in the absence of SF_6, biexponential

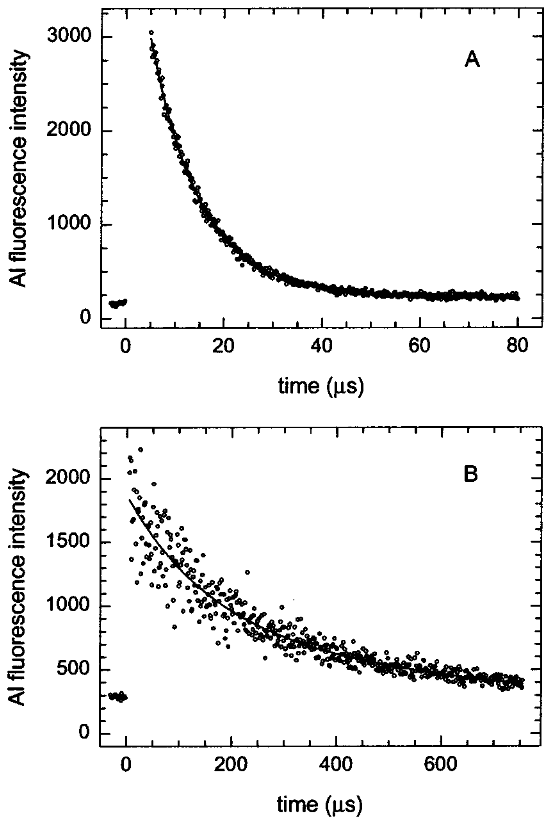

Figure 1. A: Typical Al atom decay profile when TMA was the photolytic precursor. B: Typical Al atom decay profile when TEA was the photolytic precursor. Solid lines through the data are double exponential fits.

TABLE 1: Summary of Rate Coefficient Measurements for Al + SF$_6$ → AlF + SF$_5$

T (K)	k (10^{-13} cm^3 molecule^{-1} s^{-1})	T (K)	k (10^{-13} cm^3 molecule^{-1} s^{-1})
499	0.42	666	4.9
518	0.61	693	6.7
556	1.3	721	8.6
573	2.1	723	6.9
594	3.9[a]	747	13.0
612	3.3	771	14.2
638	3.7	813	23.8

[a] Obtained by monitoring relative concentrations of AlF.

decay was observed and attributed to the equilibrium process:

$$\mathrm{Al} + \mathrm{TMA} \leftrightarrow \mathrm{Al[TMA]}.$$

At still higher temperatures ($T > 425$ K), equilibrium is established prior to our first observation and single-exponential decay is again observed with the long decay constant. Under these conditions, when SF$_6$ is added to the system, the decay is biexponential. The short time constant is due to reaction of free Al with SF$_6$, whereas the longer time constant results from the equilibrium of Al with TMA or TEA. The details of this aspect of the Al atom reaction with trialkylaluminum will be addressed in a future publication.

Table 1 lists the measured values of the bimolecular rate constants for the Al + SF$_6$ reaction obtained in this work. Thirteen of these rate constants were measured by following the disappearance of Al LIF signal while varying the partial pressure of SF$_6$. The individual decay times measured at three of the temperatures are plotted as a function of SF$_6$ pressure in Figure 2. As expected for a bimolecular reaction with a barrier, the slope of each pseudo-first-order plot increases with increasing temperature.

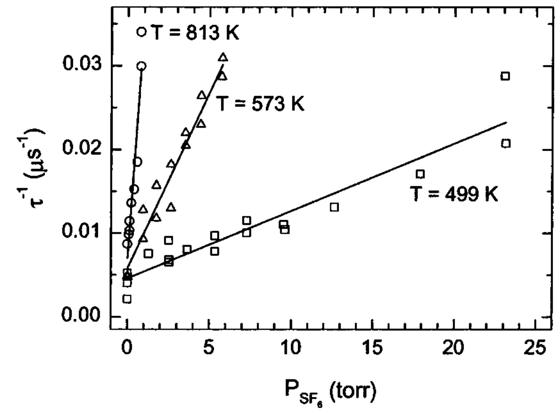

Figure 2. Linear dependence of $1/\tau$ for Al atom decay as a function of SF$_6$ partial pressure at different temperatures. P_{tot} = 100 Torr. Second-order rate constants are obtained from the slopes.

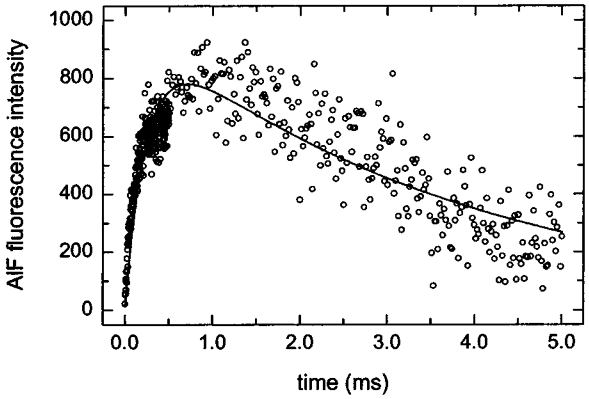

Figure 3. Kinetic behavior of AlF LIF signal over time. Solid line through the data is a double exponential fit using eq 2. P_{SF6} = 875 mTorr, P_{tot} = 100.5 Torr, and T = 594 K.

The rate constant at 594 K was measured by following formation and decay of the primary product AlF. A typical time-dependent profile for formation and decay of AlF LIF signal is shown in Figure 3. In our experiment, there were significant sources of AlF product independent of SF$_6$. The AlF profiles analyzed were the difference between profiles collected with and without added SF$_6$. For a set of coupled reactions of the form:

$$\mathrm{Al} + \mathrm{SF_6} \rightarrow \mathrm{AlF} + \mathrm{SF_5} \tag{1}$$

$$\mathrm{AlF} \rightarrow \mathrm{removal} \tag{3}$$

it can be shown[24] that

$$[\mathrm{AlF}] = \frac{[\mathrm{Al}]_0 k_1}{k_3 - k_1} \tag{4}$$

where $[\mathrm{Al}]_0$ is the concentration of aluminum atoms at $t = 0$, k_1 is the pseudo-first-order rate constant for reaction of Al with SF$_6$, and k_3 is a pseudo-first-order rate constant for removal of AlF. Reaction 3 represents disappearance of AlF by reaction with SF$_6$, aluminum atom precursor, and diffusion out of the viewing region.

By fitting the AlF formation and decay data to the double exponential expression of eq 4, the pseudo-first-order rate constants for formation and decay of AlF at eleven different partial pressures of SF$_6$ were determined. The range of SF$_6$

TABLE 2: Reaction Enthalpies, Activation Energies, and Arrhenius Preexponential Factors Calculated for the Reaction Al + $SF_6 \rightarrow AlF + SF_5$ at Various Levels of Theory

level of theory	$\Delta_r H_0$ (kcal mol^{-1})	E_a (kcal mol^{-1})	A (10^{-10} cm^3 molecule^{-1} s^{-1})
MP2/6-31G(d)	−56.2	11.1	0.81
MP2/6-311++G(2d)	−63.1	10.8	2.2
MP2/aug-cc-pVTZ//MP2/6-311++G(2d)	−57.7	13.2	2.2
BH&HLYP/6-31G(d)	−58.3	10.1	1.4
BH&HLYP/6-311++G(2d)	−64.8	9.5	1.2
BH&HLYP/aug-cc-pVTZ//BH&HLYP/6-311++G(2d)	−60.7	12.3	1.3
exptl	−68.0 ± 3.8[a]	9.5 ± 0.4	6.8 ± 2.2

[a] From ref 22.

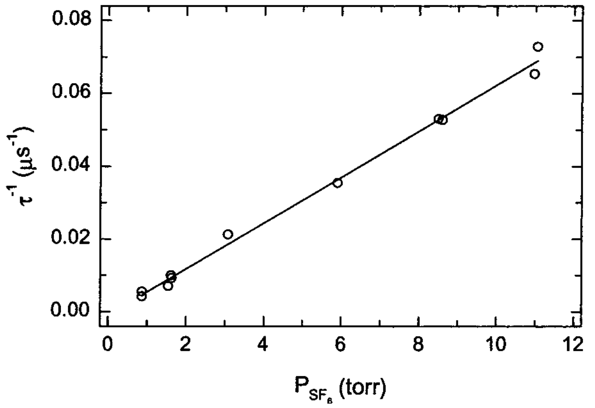

Figure 4. Linear dependence of $1/\tau$ for AlF formation as a function of SF_6 partial pressure. P_{tot} = 100 Torr.

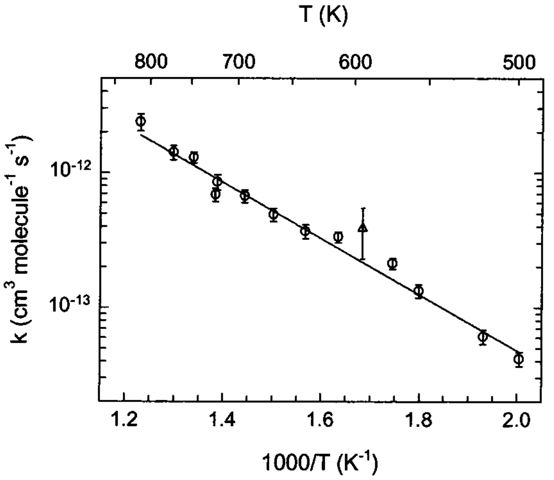

Figure 5. Arrhenius plot for Al + SF_6. The solid curve through the data represents $k(T) = 6.8\ (\pm\ 2.2) \times 10^{-10}\exp(-(4780 \pm 200\ \text{K})/T)$ cm^3 molecule^{-1} s^{-1}. Circles represent data from Al atom decays; triangle represents data from AlF formation kinetics.

partial pressure was from 0.87 to 11 Torr. A plot of the formation rate constant as a function of partial pressure of SF_6 yielded the bimolecular rate constant for reaction 1 at 594 K. This plot is shown in Figure 4. The resulting rate constant is in reasonable agreement with the rate constants obtained by monitoring Al atom decay, demonstrating that AlF is a primary product of this reaction.

The bimolecular rate constants of reaction 1 as determined from Al disappearance are plotted in Arrhenius form in Figure 5. Regression analysis yielded $k(T) = 6.8\ (\pm\ 2.2) \times 10^{-10}\exp(-(4780 \pm 200\ \text{K})/T)$ cm^3 molecule^{-1} s^{-1}. This corresponds to an activation energy of 9.5 ± 0.4 kcal mol^{-1}. Weighting factors of (uncertainty in k)$^{-2}$ were used in the fit. Also shown in Figure 5 is the rate constant determined from AlF appearance data. Errors in the measured rate constants on the Arrhenius plot were determined by adding in quadrature the independent experimental errors (assumed to be 5% for gas flow rate, 5% for temperature, 5% for pressure, and 2% for timing) and the statistical error from the pseudo-first-order plots.

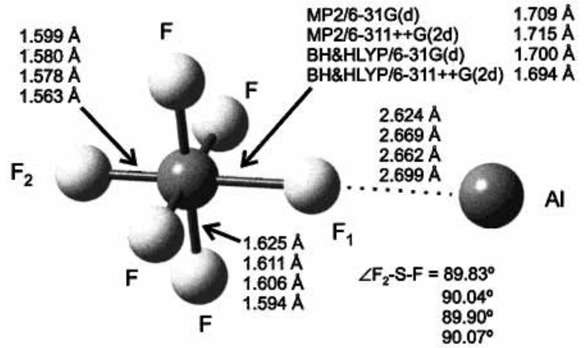

Figure 6. Calculated geometrical parameters of the Al + SF_6 atom-abstraction transition state. The molecular symmetry point group is C_{4v}.

Discussion

First, it is noted that the preexponential factor for reaction 1 is typical for atomic metatheses reactions.[25] The only other experimentally measured rate constants for the reaction of aluminum with a fluorinated species in the gas phase are those for the Al + $NF_3 \rightarrow AlF + NF_2$ reaction.[19] For this reaction, $k(T) = 2.1\ (\pm\ 0.4) \times 10^{-10}\ \exp(-(2990 \pm 100\ \text{K})/T)$ cm^3 molecule^{-1} s^{-1} over the temperature range 300−800 K. The barrier height of 2990 K corresponds to an activation energy of 5.9 kcal mol^{-1}. This is a reasonable activation energy and preexponential factor for an atom abstraction reaction and places our results for the Al + SF_6 reaction in context. Interestingly, the authors of the Al + NF_3 work were not able to get reliable kinetic information above 800 K due to decomposition of NF_3 on the walls of the reactor. As mentioned above, we had similar problems in this study.

We have computed the potential energy surface of this reaction using second-order perturbation theory with the frozen core approximation, MP2(FC), and the BH&HLYP density functional method, both with various basis sets. The BH&HLYP functional was chosen because of its known reliability in calculating barrier heights for some reactions involving fluorine.[26] We also attempted to use the more popular B3LYP functional, but a transition structure could not be located. All calculational methods for which a TS was obtained find an atom abstraction transition structure with an S−F−Al collinear bond angle. Figure 6 gives geometrical parameters of the transition state calculated at the four levels of theory. There is general agreement on the structure of the TS among the four methods used.

The results of the ab initio and DFT calculations have been used to calculate bimolecular rate constants at 500, 600, 700, and 800 K using eq 2. For each set of calculated rate constants, Arrhenius parameters were extracted. A summary of the thermokinetic computational results is provided in Table 2. The calculated structural and vibrational information for reactants, products, and the transition state of this reaction are available as Supporting Information. From Table 2 we find that the BH&HLYP/6-311++G(2d) method gives the best agreement with experiment for predicting the enthalpy of reaction and the activation energy over the experimental temperature range. In both cases, this method yields calculated parameters which are within the stated experimental uncertainty. Increasing the basis set to aug-cc-pVTZ for both BH&HLYP and MP2 methods, using single point energies from structures optimized in the 6-311++G(2d,p) basis set, moves the activation energy up (and away from the experimental value) by 2.8 and 2.4 kcal mol^{-1}, respectively. Also, the computed enthalpies of reaction at the BH&HLYP/6-311++G(2d) and MP2/6-311++G(2d) levels of theory move up and out of the range of experimental uncertainty when the aug-cc-pVTZ basis set is used. These trends, which are independent of correlation method, suggest that reoptimization of structures may be important when moving to the aug-cc-pVTZ basis set. We attempted to optimize the transition state structure from the BH&HLYP/6-311++G(2d,p) level at the BH&HLYP/aug-cc-pVTZ level of theory but the calculation failed due to our lack of computational resources.

The MP2/6-311++G(2d) method gives an Arrhenius preexponential factor in closest agreement with experiment. However, all methods underestimate the A-factor for this reaction. The simplest explanation for the small calculated A-factors is that the calculated transition structure is too “tight”. A looser transition state would mean a longer Al···S distance, which would lead to an increase in the moments of inertia of the TS. This would increase the value of the rotational partition function. Also, a looser TS would tend to decrease the values of the lowest lying vibrational mode (bending mode, E symmetry), causing the vibrational partition function of the TS to increase, thereby increasing the A-factor.

Summary

The rate constants of the reaction of Al + SF_6 were measured between 499 and 813 K at 100 Torr total pressure. The reaction proceeds through an atom abstraction transition state with an activation barrier of 9.5 ± 0.4 kcal mol^{-1}. Calculated rate constants at the BH&HLYP/6-311++G(2d) level of theory are in good agreement with experiment.

Acknowledgment. We thank A. P. Baronavski and T. Russell for helpful discussions. We also thank A. D. Berry for help in handling and transfer of aluminum alkyl reagents, and H. D. Ladouceur for help in reactor design. This work was supported by the Office of Naval Research through the Naval Research Laboratory and was performed while J. K. Parker held a National Research Council—Naval Research Laboratory Associateship.

Supporting Information Available: Structural and vibrational information for reactants, products, and the transition state of the Al + SF_6 → AlF + SF_5 reaction from the ab initio and DFT calculations. This material is available free of charge via the Internet at http://pubs.acs.org.

References and Notes

(1) Sutton, G. P. *Rocket Propulsion Elements*; John Wiley & Sons: New York, 1992.

(2) Peretz, A. Some Theoretical Considerations of Metal-Fluorocarbon Compositions for Ramjet Fuels. Presented at the 8th International Symposium on Air Breathing Engines, Cincinnati, OH, June 14−19, 1987.

(3) Yetter, R. A.; Dryer, F. L.; Rabitz, H.; Brown, R. C., Kolb, C. E. *Combust. Flame* **1997**, *112*, 389.

(4) Farber, M.; Srivastava, R. D. *Combust. Flame* **1976**, *27*, 99.

(5) Ernst, L. F.; Dryer, F. L.; Yetter, R. A.; Parr, T.; Hanson-Parr, D. M. *Proceedings of the 36th JANNAF Combustion Subcommittee Meeting*, 1999.

(6) Feler, W. Technical Report Prepared for Air Force Office of Scientific Research, AFOSR-TR-0599, 1981.

(7) Beuermann, Th.; Stuke, M. *Chem. Phys. Lett.* **1991**, *178*, 197.

(8) Garland, N. L.; Douglass, C. H.; Nelson, H. H. *J. Phys. Chem.* **1992**, *96*, 8390.

(9) Mithchell, S. A.; Hackett, P. A.; Rayner, D. M.; Cantin, M. *J. Phys. Chem.* **1986**, *90*, 6148.

(10) Frisch, M. J.; Trucks, G. W.; Schlegel, H. B.; Scuseria, G. E.; Robb, M. A.; Cheeseman, J. R.; Zakrzewski, V. G.; Montgomery, J. A., Jr.; Stratmann, R. E.; Burant, J. C.; Dapprich, S.; Millam, J. M.; Daniels, A. D.; Kudin, K. N.; Strain, M. C.; Farkas, O.; Tomasi, J.; Barone, V.; Cossi, M.; Cammi, R.; Mennucci, B.; Pomelli, C.; Adamo, C.; Clifford, S.; Ochterski, J.; Petersson, G. A.; Ayala, P. Y.; Cui, Q.; Morokuma, K.; Malick, D. K.; Rabuck, A. D.; Raghavachari, K.; Foresman, J. B.; Cioslowski, J.; Ortiz, J. V.; Baboul, A. G.; Stefanov, B. B.; Liu, G.; Liashenko, A.; Piskorz, P.; Komaromi, I.; Gomperts, R.; Martin, R. L.; Fox, D. J.; Keith, T.; Al-Laham, M. A.; Peng, C. Y.; Nanayakkara, A.; Gonzalez, C.; Challacombe, M.; Gill, P. M. W.; Johnson, B.; Chen, W.; Wong, M. W.; Andres, J. L.; Gonzalez, C.; Head-Gordon, M.; Replogle, E. S.; Pople, J. A. *Gaussian 98*, Revision A.7; Gaussian, Inc.: Pittsburgh, PA, 1998.

(11) Lee, C.; Yang, W.; Parr, R. G. *Phys Rev. B* **1988**, *37*, 785.

(12) Becke, A. D. *J. Chem. Phys.* **1993**, *98*, 1372.

(13) Møller, C.; Plesset, M. S. *Phys. Rev.* **1934**, *46*, 618.

(14) Ditchfield, R.; Hehre, W. J.; Pople, J. A. *J. Chem. Phys.* **1971**, *54*, 724.

(15) Hariharan, P. C.; Pople, J. A. *Theor. Chim. Acta* **1973**, *28*, 213.

(16) Krishnan, R.; Binkley, J. S.; Seeger, R.; Pople, J. A. *J. Chem. Phys.* **1980**, *72*, 650.

(17) Frisch, M. J.; Pople, J. A.; Binkley, J. S. *J. Chem. Phys.* **1984**, *80*, 3265.

(18) Dunning, T. H. *J. Chem. Phys.* **1989**, *90*, 1007.

(19) Szabo, A.; Ostlund, N. S. *Modern Quantum Chemistry*; Dover Publications: Mineola, NY, 1989.

(20) Eyring, H. *J. Chem. Phys.* **1935**, *3*, 107.

(21) Truhlar, D. G.; Hase, W. L.; Hynes, J. T. *J. Phys. Chem.* **1983**, *87*, 2664.

(22) Chase, M. W., Jr.; Davies, C. A.; Downey, J. R., Jr.; Frurip, D. J.; McDonald, R. A.; Syverud, A. N. *J. Phys. Chem. Ref. Data* **1985**, 14.

(23) Parnis, J. M.; Mitchell, S. A.; Kanigan, T. S.; Hackett, P. A. *J. Phys. Chem.* **1989**, *93*, 8045.

(24) Frost, A. A; Pearson, R. G. *Kinetics and Mechanism*, 2nd ed.; John Wiley & Sons: New York, 1961.

(25) Benson, S. W. *Thermochemical Kinetics*; John Wiley & Sons: New York, 1976.

(26) Lynch, B. J.; Truhlar, D. G. *J. Phys. Chem. A* **2001**, *105*, 2936.